Available online at www.sciencedirect.com
SCIENCE DIRECT®
International Journal of Heat and Mass Transfer 47 (2004) 2949–2959
International Journal of HEAT and MASS TRANSFER
www.elsevier.com/locate/ijhmt

Cluster potentials for multi-scale interactions

D.Y. Tzou [a,*], J.K. Chen, R. Roybal, J.E. Beraun [b]

[a] Department of Mechanical and Aerospace Engineering, University of Missouri-Columbia, Columbia, MO 65211, USA
[b] Laser Effects Research Branch, Directed Energy Directorate, Air Force Research Laboratory, Kirtland AFB, NM 87117, USA

Received 20 June 2003; received in revised form 15 March 2004

Abstract

A cluster approach has been proposed to describe the process of heat transport in microscale. Molecular clustering is described by integrating the Lennard-Jones potential over specific physical domains, forming cluster potentials that possess repulsive and attractive forces sensitively varying with the geometrical shapes of the molecular clusters. The cluster potentials thus developed provides a consistent approach for describing multi-scale heat transport, in that different shapes/dimensions of the clusters take different exponents in the repulsive and attractive forces. A one-dimensional example is given to illustrate the essence of the cluster dynamics simulation, emphasizing devious behavior from molecular motion and replacement of a physical boundary by the cluster potential of a different scale.

1. Introduction

A small-scale device, unlike the large-scale devices containing millions of molecules, is composed of a limited number of molecules. The 0.1 μm film employed for studying ultrafast heat transport in femtosecond laser heating [1–6], for example, contains only thousands of molecules that have limited capabilities in conducting heat or transmitting load. As a result, thermal conductivity (measuring the energy-bearing capacity) and elastic moduli (measuring the load-carrying capacity) of the small-scale device may be very different from those of the large-scale device made of the same materials.

Molecular dynamics (MD) simulation has been proven effective in modeling the process of heat transport in microscale [7–9]. Most recently, in 1996, a two-volume symposium [10] was published that summarizes the use of MD simulations in microscale processing, solidification, as well as prediction of microscale thermophysical properties and modeling of microstructured surfaces. A thorough review on the MD simulation became available in 1999 [11], which covers a wider spectrum of MD simulations including the use of normal and modified Lennard-Jones (LJ) potentials for gases and liquids, Stillinger and Weber [12] and Tersoff [13] potentials for silicon, and the ab initio MD method that considers electronic states by using the Schrödinger wave equation as the equation of motion to address the quantum-mechanical effects [14,15]. MD simulation describes the individual behavior of molecules by solving a large set of coupled equations of motion that bridges all molecules together, with the gradient of the molecular potential serving as the driving forces. Thermomechanical responses, including temperature, heat flux vector, and stress can then be evaluated based on the statistical averages involving molecular positions, velocities, and energies in accordance with the virial theorem [16,17], for example. Symmetric conditions are usually required at the boundaries of the computational cells, implying a repetitive response of the molecular assembly in transition from one cell to another. The number of molecules involved in the computational cell ranges from hundreds (10^2) to 10^6, depending on the complexity of the targeted behavior in the microsystem. As the number of molecules increases in the computational cell, to keep computational time manageable, the cutoff radius is usually introduced in describing the intermolecular potential.

* Corresponding author. Tel.: +1-573-882-4060; fax: +1-573-884-5090.
E-mail address: tzour@missouri.edu (D.Y. Tzou).

0017-9310/$ - see front matter © 2004 Elsevier Ltd. All rights reserved.
doi:10.1016/j.ijheatmasstransfer.2004.03.019

Nomenclature

a, b	radii of spheres (m)
A	constant in the general form of cluster potential
c	central distance (m)
C_1	constant in LJ potential ($\mathrm{J\,m^{12}}$)
C_2	constant in LJ potential ($\mathrm{J\,m^{6}}$)
d	distance between surfaces
E	cluster potential (J)
F	force (N)
m, n	number densities of molecules ($1/\mathrm{m^3}$)
N_1, N_2	constants in the general form of cluster potential
r	distance (m)
R	distance between the cluster center and the representative plane (m)
U	molecular potential (J)
x	radius of disks (m)
y	distance between molecule and the representative point (m)
y'	distance between molecule and the cluster center (m)

Greek symbols

θ	polar angle (rad)
ρ	radial distance (m)

Subscripts and superscripts

D–S	disk-to-sphere
LJ	Lennard-Jones
M–D	molecule-to-disk
S–S	sphere-to-sphere
i, j	molecule i and j
0	equilibrium
2D	two-dimensional
3D	three-dimensional
*	nondimensional quantities

The cutoff radius for the LJ potential, for example, is roughly 2.6σ [7], with $(2^{1/6}\sigma)$ being the position of mechanical equilibrium at which the intermolecular force is zero.

Beyond the already-complicated individual molecules, complex systems in microscale may involve molecular clusters of various shapes [18,19]. An example would be the nano-diode made of nanotubes with hexagonal clusters uniformly distributed on the circumference. The hexagonal clusters are formed by joining an even rolled graphite sheet (with semiconducting behavior) to a spiral rolled sheet (metallic behavior). Hundreds of thousands of molecules may be needed to model just one hexagonal cluster, making it extremely difficult to predict the functional behavior of a single nanotube where hundreds of thousands of such hexagonal clusters are present. Creation of functional nanomaterials poses the same challenge [20]. As hundreds of thousands of nanophase agglomerates are collected from a liquid-hydrogen cooled tube, with tens and hundreds of molecules involved in each agglomerate, interactions among such agglomerates, rather than the individual molecules, would dominate the functionalities of the consolidated (sintered) nanophase materials. Conventional MD simulation should be able to characterize the thermophysical properties for such complex systems, at least in principle, but the numerical efforts will be immense. In the continuous expansion of the MD simulation capabilities, therefore, there is a need for branching our efforts into modeling the dynamics of the preformed clusters.

Aiming at the complex system consisting of nanophase assemblies as the building blocks, the present work develops the cluster interaction potentials for describing the physical behavior of complex microsystem. The well-known LJ potential is used as the Green's function to derive the new potentials as numerous molecules are clustered in various shapes, under the assumption that the number of molecules involved each cluster is sufficient large to produce a uniform distribution. It is shown that the exponents characterizing the repulsive and attractive forces sensitively vary with the cluster shapes, with the case of a nano-surface specially derived to replace the symmetric boundary conditions assumed in traditional MD simulation. One-dimensional study follows, aiming at special characteristics of cluster dynamics, as well as dynamic modeling involving clusters/molecules at different scales.

2. Cluster potentials

Lennard-Jones potential is one of the most popular models used in the MD simulation due to its simple form and well-tabulated parameters for different materials:

$$U_{ij}(r_{ij}) = \frac{C_1}{r_{ij}^{12}} - \frac{C_2}{r_{ij}^{6}}; \quad F_{ij} = -\frac{\mathrm{d}U_{ij}}{\mathrm{d}r_{ij}} = \frac{12C_1}{r_{ij}^{13}} - \frac{6C_2}{r_{ij}^{7}} \tag{1}$$

The equilibrium position $(r_{ij}^{(0)})$ is obtained from $F_{ij} = 0$, or $r_{ij}^{(0)} = (2C_1/C_2)^{1/6}$. As the two molecules are close, at a distance smaller than $r_{ij}^{(0)}$, the repulsive force activates and is characterized by the exponent 12. As the two

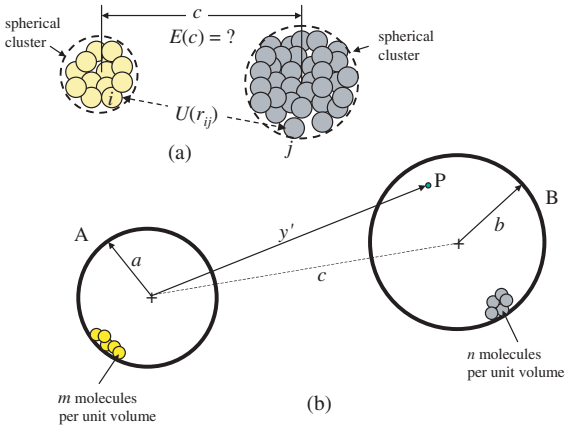

Fig. 1. Spherical clusters composed of uniformly compacted molecules. (a) Cluster potentials $E(c)$ resulting from the LJ potential (U) exerting on any pair of molecules (i and j) in each cluster. (b) Interaction potential between spherical clusters and their relative positions.

molecules are far apart, at any distance greater than $r_{ij}^{(0)}$, the attractive force galvanizes and is characterized by the exponent 6. Typical values of C_1 and C_2 are of the order of 10^{-26} (J nm^{12}) and $C_2 = 10^{-23}$ (J nm^6), respectively [7,8].

A cluster defined in this work is an assembly of molecules that are compacted uniformly in a physical domain of a certain shape. It can be viewed as ad Its physical size may be two to three orders of magnitude greater than a molecule (measured in angstroms), but the overall dimension remains in nanoscale, from nanometers to submicrons. The interaction potential between any pair of molecules, which are represented by i and j in Fig. 1(a), is the LJ potential shown by Eq. (1). As these molecules congregate and form clusters of specific shapes, the major task is determination of the *cluster potential*, represented by $E(c)$ in Fig. 1(a), with c being the distance between two clusters. Fig. 1(b) shows two spherical clusters, A and B of radii a and b, respectively, with the central distance denoted by c. Molecules in each spherical cluster are assumed numerous, uniformly distributed throughout with the number densities of m (in Sphere A) and n (in Sphere B).

2.1. Molecule-to-sphere potential

Consider a representative molecule in Sphere B, denoted by point P in Fig. 1(b), which interacts with all the molecules in Sphere A. The coordinate system employed for deriving the resulting molecule-to-sphere potential is illustrated in Fig. 2, where a representative disk of thickness dr is further extracted from A to derive the molecule-to-disk potential, as the first step. Lennard-Jones potential exerts between P and the infinitesimal

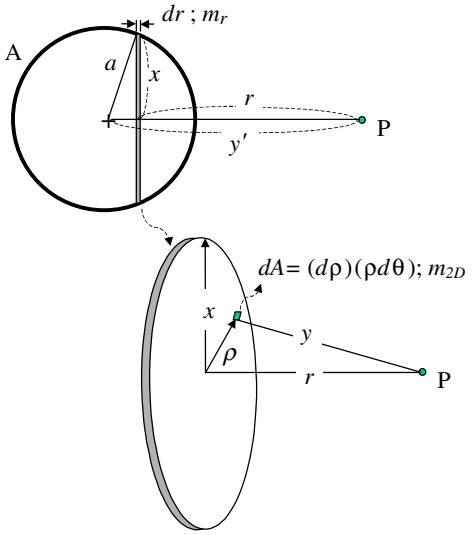

Fig. 2. Representative disk of differential thickness dr in Sphere A and the planar coordinate system. Number density of molecules in the r-direction, m_r, and that over the disk, m_{2D}.

area $\mathrm{d}A(=\rho\,\mathrm{d}\rho\,\mathrm{d}\theta)$ on the disk. With $y = (\rho^2 + r^2)^{1/2}$ in place of r_{ij} in Eq. (1) and integrating the LJ potential, now becoming $U(y)$ with $i \equiv P$ and $j \equiv \mathrm{d}A$, over the entire disk of radius x, the two-dimensional interaction potential between P and the disk is

$$E_{\mathrm{M-D}}(x,r) = m_{2\mathrm{D}} \int_0^x U(y)|_{y=\sqrt{\rho^2+r^2}} \cdot \rho\,\mathrm{d}\rho \int_0^{2\pi} \mathrm{d}\theta = 2\pi m_{2\mathrm{D}} \left\{ C_1 \left[\frac{1}{10r^{10}} - \frac{1}{10(r^2+x^2)^5} \right] - C_2 \left[\frac{1}{4r^4} - \frac{1}{4(r^2+x^2)^2} \right] \right\} \tag{2}$$

where $m_{2\mathrm{D}}$ measures the number of molecules per unit area on the disk. In the limiting case that P is very close to the disk, $r \to 0$, the asymptotic form of Eq. (2) is

$$\lim_{r\to 0} E_{M-D} \cong 2\pi m_{2\mathrm{D}} \left(\frac{C_1}{10r^{10}} - \frac{C_2}{4r^4} \right) \quad \text{(molecular-to-disk)} \tag{3}$$

Though having a much more complicated form in general, the repulsive and attractive indices in the molecular-to-disk potential sensitively change to the 10–4 relation, in contrast to the original 12–6 (LJ) relation, as the distance between P and the disk is small $(r \to 0)$. Integrating $E_{\mathrm{M-D}}$ in Eq. (2) for a disk of thickness (dr) over the entire sphere with r ranging from $(y' - a)$ to $(y' + a)$ and instating the relation of $x^2 = [a^2 - (y' - r)^2]$ in the integrand, the molecule-to-sphere potential follows,

$$E_{\text{M-S}}(y') = \int_{y'-a}^{y'+a} E_{\text{M-D}}(x,r)\big|_{x=\sqrt{a^2-(y'-r)^2}} \cdot m_r \,\mathrm{d}r$$
$$= 2\pi m\left\{C_1\left[\frac{1}{90d^9} - \frac{1}{(80a)d^8} + \frac{1}{(80a^2)d^7} - \cdots - \frac{2299}{184320a^9} + \left(\frac{253}{20480}\right)d + \cdots\right] - C_2\left[\frac{1}{12d^3} - \frac{1}{(8a)d^2} + \frac{1}{(8a^2)d} - \frac{5}{48a^3} + \left(\frac{5}{64a^4}\right)d + \cdots\right]\right\} \quad (4)$$

where $m = (m_r \cdot m_{2\text{D}})$ recovers the number density of molecules per unit volume and the Taylor series expansion in terms of $d = (y' - a)$, the distance between P and the *surface* of Sphere A, has been applied to reveal the asymptotic behavior of $E_{\text{M-S}}$ as the value of d becomes small. In the limit of $d \to 0$, clearly,

$$\lim_{d\to 0} E_{\text{M-S}} \cong \pi m\left(\frac{C_1}{45d^9} - \frac{C_2}{6d^3}\right). \quad \text{(molecule-to-sphere)} \quad (5)$$

The 10–4 relation further evolves into the 9–3 relation in transit from the molecule-to-disk potential (Eq. (3)) to the molecule-to-sphere potential (Eq. (5)).

Before continuing on, note that the LJ potential has been used as the Green's function in deriving the molecule-to-disk and the molecule-to-sphere potentials. The process is identical to that in deriving the temperature solution for area heating from the temperature solution for a point heat source.

2.2. Sphere-to-sphere potential

The molecule-to-sphere potential derived in Eq. (4) now serves as the Green's function in describing the sphere-to-sphere interaction, as illustrated in Fig. 3. The molecule-to-sphere potential, $E_{3\text{D}}$ in Eq. (4), exists between Sphere A and $\mathrm{d}A'$ over the distance y'. The infinitesimal area $\mathrm{d}A'(= \rho'\,\mathrm{d}\rho'\,\mathrm{d}\theta')$ is in place of the previous representative point P, which is located on the representative disk of thickness $\mathrm{d}R$ in Sphere B. Replacing y' in Eq. (4) by $(\rho'^2 + R^2)^{1/2}$ and integrating $E_{\text{M-S}}$ (the full form) over the entire disk with $\rho' \in [0, x']$ and $\theta' \in [0, 2\pi]$, similarly, the disk-to-sphere potential ($E_{\text{D-S}}$) can be obtained from

$$E_{\text{D-S}}(x') = n_{2\text{D}} \int_0^{x'} E_{\text{M-S}}(y')\big|_{y'=\sqrt{\rho'^2+R^2}} \cdot \rho'\,\mathrm{d}\rho' \int_0^{2\pi} \mathrm{d}\theta' \quad (6)$$

The asymptotic result limit with $d \to 0$, where $d(= R - a)$ represents the distance from the center of the disk to the surface of Sphere A, Eq. (6) gives

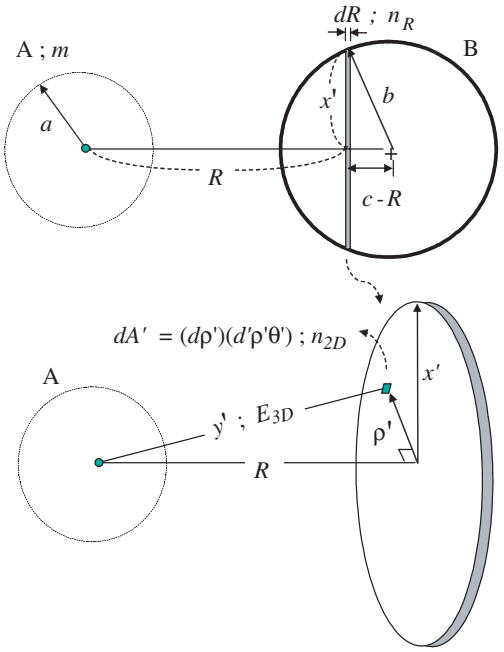

Fig. 3. Relative coordinates between two spherical clusters and the use of $E_{3\text{D}}$ as the Green's function in deriving the sphere-to-sphere potential.

$$\lim_{d\to 0} E_{\text{D-S}} \cong \pi^2 m \cdot n_{2\text{D}} a\left(\frac{C_1}{180d^8} - \frac{C_2}{6d^2}\right) \quad \text{(disk-to-sphere)} \quad (7)$$

The terms containing x' are all dropped out in the case of $d \to 0$, because the sphere (of radius a) is very close to the disk (of radius x'). In Eq. (7), $n_{2\text{D}}$ is the number density of molecules per unit area on the disk (of thickness $\mathrm{d}R$) located within Sphere B. The 9–3 relation (molecule-to-sphere potential) has evolved into the 8–2 relation (disk-to-sphere potential). Integrating the *full form* of $E_{\text{D-S}}$ the one containing all terms in x' now replaced by $[b^2 - (c-R)^2]^{1/2}$, in the domain of R from $(c-b)$ to $(c+b)$, we have the sphere-to-sphere potential:

$$E_{\text{S-S}} = \pi^2 mn\left[C_1\left(\frac{ab}{1260(a+b)d^7} - \frac{a^2+8ab+b^2}{7560(a+b)^2d^6} + \cdots\right) - C_2\left(\frac{ab}{6(a+b)d} - 0(d^0) + \cdots\right)\right] \quad (8)$$

where $n = n_{2\text{D}} \times n_R$ has been replaced and $d = c - a - b$ refers to the distance between the surfaces of two spheres. In the asymptotic limit of $d \to 0$, likewise,

$$\lim_{d\to 0} E_{\text{S-S}} \simeq \frac{\pi^2 abmn}{a+b}\left[\frac{C_1}{1260d^7}-\frac{C_2}{6d}\right] \quad \text{(sphere-to-sphere)} \tag{9}$$

For nanoscale clusters of the same size ($b=a$) and number densities ($n=m$), in particular,

$$\lim_{d\to 0} E_{\text{S-S}} \simeq \pi^2 m^2 a\left[\frac{C_1}{2520d^7}-\frac{C_2}{12d}\right] \quad \text{(identical spheres)} \tag{10}$$

The 8–2 relation for the disk-to-sphere potential finally evolves into the 7–1 relation for the sphere-to-sphere potential, which is equivalent to the symbol $E(c)$ employed in Fig. 1(a) as the two interacting clusters take the form of spheres.

A crack tip in a continuum could be viewed as the location where two clusters join together, separating at a distance in which the attractive force prevails. Such a distance cannot enter the repulsive regime because the continuum concept used in stress analysis. The component of the attractive force derived in Eq. (10), $(\pi m)^2 aC_2/(12d) \sim 1/d$, nicely captures the well-known $(1/d)$ behavior of the strain energy density function [21,22], which is a special form of potential energy in lattice structures, regardless of different types of the constitutive relations established on the macroscale level [23,24]. Such a $1/d$-behavior is an intrinsic behavior that has also been found in flow potentials and Biot energy near the singularities in thermal and flow fields [25].

2.3. Other geometry

Eqs. (2)–(10) demonstrate the ways in which the 12–6 (LJ) intermolecular potential evolves into the 7–1 cluster potential as the nano-species evolve from molecules to spheres. Geometrical evolution from a point (molecule), a disk, to a sphere implies participation of clusters of various shapes crossing several orders of magnitude in physical scales. In modeling the multi-scale interaction effects via the cluster potential thus developed, this would involve a simple change of the indices (12–6 or 7–1) reflecting the shape-dependent, and hence the scale-dependent, repulsive and attractive forces.

Table 1 summarizes the asymptotic cluster potentials assuming a small distance d. The cluster forces result from the spatial derivative of the cluster potential with respect to d and the mechanical equilibrium positions result from the value of d at which the cluster forces vanish. In all cases, the difference between the repulsive (12 in the LJ potential) and attractive (6) indices always keeps at six (6). Both repulsive and attractive indices decrease as the dimensionalities of the participating clusters increase. For cluster geometry involving a molecule (point, dimension 0) or a nanowire (line, dimension 1), for example, both repulsive and attractive indices reduce by a number that is the sum of the *total dimensions* of the participating clusters. The molecule-to-nanosurface (dimension 2) potential, for instance, reduces the repulsive index from 12 (molecule-to-molecule) to $12-(2+0)=10$. Exceptions may exist for

Table 1
Asymptotic results of cluster potentials, forces, and equilibrium positions

Clusters types	Cluster potentials	Cluster forces	Equilibrium positions
Molecule-to-molecule	$\frac{C_1}{d^{12}}-\frac{C_2}{d^6}$	$\frac{12C_1}{d^{13}}-\frac{6C_2}{d^7}$	$\left(\frac{2C_1}{C_2}\right)^{1/6}$
Molecule-to-nanowire (semiinfinite)	$\pi m_{1\text{D}}\left(\frac{63C_1}{512d^{11}}-\frac{3C_2}{16d^5}\right)$	$\pi m_{1\text{D}}\left(\frac{693C_1}{512d^{12}}-\frac{15C_2}{16d^6}\right)$	$\left(\frac{231C_1}{160C_2}\right)^{1/6}$
Molecule-to-nanowire (infinite)	$\pi m_{1\text{D}}\left(\frac{63C_1}{256d^{11}}-\frac{3C_2}{8d^5}\right)$	$\pi m_{1\text{D}}\left(\frac{693C_1}{256d^{12}}-\frac{15C_2}{8d^6}\right)$	$\left(\frac{231C_1}{160C_2}\right)^{1/6}$
Nanowires	$\pi m_{1\text{D}}^2\left(\frac{C_1}{5d^{10}}-\frac{C_2}{2d^4}\right)$	$2\pi m_{1\text{D}}^2\left(\frac{C_1}{d^{11}}-\frac{C_2}{d^5}\right)$	$\left(\frac{C_1}{C_2}\right)^{1/6}$
Molecule-to-nanosurface	$\pi m_{2\text{D}}\left(\frac{C_1}{5d^{10}}-\frac{C_2}{2d^4}\right)$	$2\pi m_{2\text{D}}\left(\frac{C_1}{d^{11}}-\frac{C_2}{d^5}\right)$	$\left(\frac{C_1}{30C_2}\right)^{1/6}$
Molecule-to-sphere	$\pi m\left(\frac{C_1}{45d^9}-\frac{C_2}{6d^3}\right)$	$\pi m\left(\frac{C_1}{5d^{10}}-\frac{C_2}{2d^4}\right)$	$\left(\frac{2C_1}{5C_2}\right)^{1/6}$
Disk-to-sphere	$\pi m n_{2\text{D}} a\left(\frac{C_1}{180d^8}-\frac{C_2}{6d^2}\right)$	$\pi m n_{2\text{D}} a\left(\frac{2C_1}{45d^9}-\frac{C_2}{3d^3}\right)$	$\left(\frac{2C_1}{15C_2}\right)^{1/6}$
Spheres (identical)	$\pi^2 m^2 a\left(\frac{C_1}{2520d^7}-\frac{C_2}{12d}\right)$	$\pi^2 m^2 a\left(\frac{C_1}{360d^8}-\frac{C_2}{12d^2}\right)$	$\left(\frac{C_1}{30C_2}\right)^{1/6}$
Sphere-to-nanosurface (infinite)	$\pi^2 m n_{2\text{D}} a\left(\frac{C_1}{1260d^7}-\frac{C_2}{6d}\right)$	$\pi^2 m n_{2\text{D}} a\left(\frac{C_1}{180d^8}-\frac{C_2}{6d^2}\right)$	$\left(\frac{C_1}{30C_2}\right)^{1/6}$

clusters involving finite 2D (disks) or 3D (spheres) geometries. In this case, the rule is to add one (1) to the result due to the additional integration performed in the polar direction. In the disk-to-sphere potential, for example, the repulsive index is $12-(2+3)+1=8$ whereas the attractive index is $8-6=2$. Such a nice feature results from the polynomial form of the LJ potential and the processes of progressive integrations as the dimensionality of the participating cluster increases.

The results shown in Table 1 suggests the following form for the general expression of the cluster potential,

$$E(d)=A\left(\frac{C_1}{N_1 d^m}-\frac{C_2}{N_2 d^n}\right) \tag{11}$$

Except for C_1 and C_2, which are intrinsic constants in the intermolecular (LJ) potential, all coefficients and indices are cluster-shape dependent. For spherical clusters, as an example, $A=(\pi m)^2 a$, $N_1=2520$, $N_2=12$, $m=7$ and $n=1$. In molecule-to-molecule interactions, as another example, $A=1$, $N_1=1$, $N_2=1$, $m=12$ and $n=6$. While N_1, N_2, m, and n are shape-dependent constants, coefficient A always depends on the characteristic length of the cluster (such as radius a for a spherical cluster) and the number density of molecules included in the cluster. Eq. (11) can be made nondimensional by introducing the potential-well-depth (E_0) at the equilibrium distance (d_0):

$$\frac{\mathrm{d}E(d)}{\mathrm{d}(d)}=0 \quad \text{at} \quad d=d_0, \quad E(d_0)=-E_0 \quad (E_0>0) \tag{12}$$

Eq. (11) then becomes

$$E^*=\frac{E}{E_0}=\frac{1}{6}\left(\frac{n}{D^m}-\frac{m}{D^n}\right),$$

$$\text{with} \quad D=\frac{d}{d_0}, \quad \text{and consequently,}$$

$$F=-\frac{\mathrm{d}E}{\mathrm{d}(d)}$$

$$\Rightarrow F^*=\frac{F}{(E_0/d_0)}=\frac{mn}{6}\left(\frac{1}{D^{m+1}}-\frac{1}{D^{n+1}}\right) \quad \text{(clusters)} \tag{13}$$

where in terms of the parameters A, N_1, N_2, m, and n in the cluster potential,

$$d_0=\left(\frac{mN_2C_1}{nN_1C_2}\right)^{1/6}, \quad E_0=\frac{6AC_1}{nN_1}\left(\frac{mN_2C_1}{nN_1C_2}\right)^{-m/6} \tag{14}$$

In the case of the LJ potential, $A=1$, $N_1=1$, $N_2=1$, $m=12$ and $n=6$, the reference values become

$$d_{0,\mathrm{LJ}}=\left(\frac{2C_1}{C_2}\right)^{1/6}, \quad E_{0,\mathrm{LJ}}=\frac{C_2^2}{4C_1} \tag{15}$$

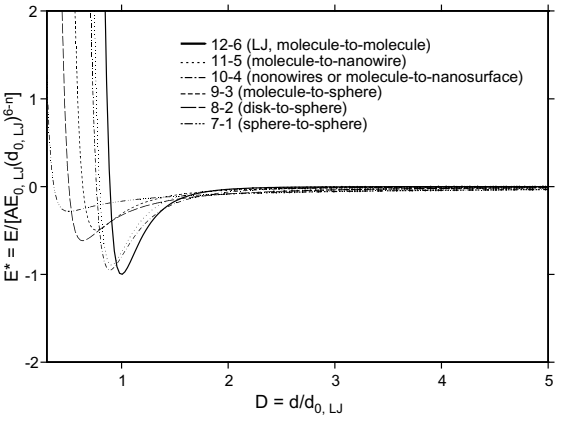

Fig. 4. Comparison of the cluster potentials with the LJ potential based on $d_{0,\mathrm{LJ}}$ and $E_{0,\mathrm{LJ}}$.

Fig. 4 displays the cluster potentials, Eq. (13), normalized on the same bases of $d_{0,\mathrm{LJ}}$ and $E_{0,\mathrm{LJ}}$ Generally speaking, the cluster potential has a shorter equilibrium distance than the L-J potential, due to the larger mass of the cluster as molecules congregate into various shapes. Both the potential-well-depth and the equilibrium position decrease as the value of m and n decreases, which implies increase of the dimensionality of the cluster.

Based on the equilibrium values in each potential, as defined by d_0 and E_0 in Eq. (14), Fig. 5 displays the cluster potentials and forces for clusters with increasing dimensionalities, i.e., the values of m and n. While maintaining similar behaviors in the repulsive regime $(D<1)$, in terms of the more gradual change of the cluster potential (left) and the lower peak and the broader distribution of the cluster forces (right), clusters of higher dimensions (such as the case of sphere-to-sphere) behave more smoothly in the attractive regime $(D>1)$ due to the stronger cumulative behavior over more molecules in the clusters. The interaction force between two molecules (LJ-potential) vanishes as the distance between two molecules exceeds approximately $2.6d_0$, $d>2.6d_0$, which coincides with the threshold value of the cutoff radius employed in Refs. [7,8] for improving the numerical efficiency. The cluster of higher dimensions, on the other hand, has a longer range of influence, with the effective distance (d) extending well beyond $7d_0(d>7d_0)$ Numerically, this implies a longer computational time when employing the cluster model in simulating the functional nanophase materials.

The asymptotic potential shown in Eq. (13) represents the dominating terms as the distance between adjacent clusters is small $(d\to 0)$. For identical spheres $(a=b)$, the general expression of the nondimensional

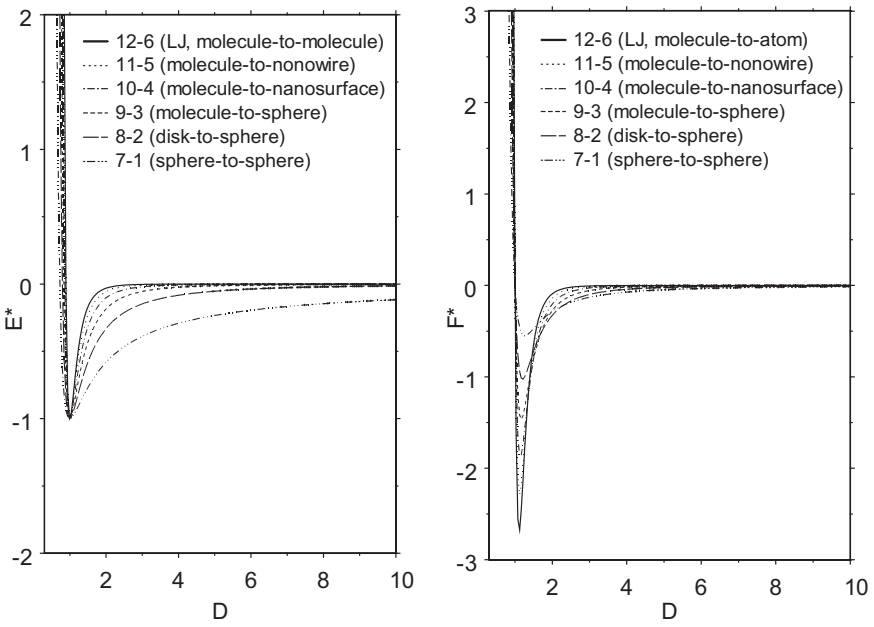

Fig. 5. Comparisons of potentials (left) and forces (right) for clusters of various shapes based on $d_0(D = d/d_0)$ and $E_0(E^* = E/E_0)$ in Eq. (14).

potential involves both the nondimensional radius $(A = a/d_0)$ and surface distance $(D = d/d_0)$:

$$
\begin{aligned}
E^*_{\text{S-S}} &= \frac{1}{9450AD^7(2A+D)^8(4A+D^7)} \\
&\times \Big\{ -2A^2\big[859,320A^3D^{17} + 77,070A^2D^{18} + 4200AD^{19} \\
&+ 105D^{20} + 7,864,320A^{14}(-1+7D^6) \\
&+ 655,360A^{13}D(-59+546D^6) + 6720A^5D^9 \\
&\times (-25+5244D^6) \\
&+ 840A^4D^{10}(-10+7737D^6) \\
&+ 57,344A^{11}D^3(-2009+30,600D^6) \\
&+ 32,768A^{12}D^2(-2633+31,395D^6) \\
&+ 13,440A^7D^7(-584+31,523D^6) \\
&+ 3360A^6D^8 \times (-446+42,005D^6) \\
&+ 14,336A^{10}D^4(-7117+139,365D^6) \\
&+ 10,752A^9D^5 \times (-5821+150,090D^6) \\
&+ 2688A^8D^6(-9967+355,865D^6)\big] \\
&+ 105D^7(2A+D)^8 \times (4A+D)^7 \\
&\times \left[\tanh^{-1}\left(1+\frac{D}{A}\right) - \tanh^{-1}\left(3+\frac{D}{A}\right)\right]\Big\} \qquad (16)
\end{aligned}
$$

The asymptotic expression, Eq. (13) with $m = 7$ and $n = 1$ for identical spheres, is a close approximation in the full rage of D as A becomes large $(A > 50)$. Under a smaller value of A, say $A = 10$ or $a = 10d_0$, the asymptotic potential is greater than the full potential but less than 20 percent, which mainly occurs in $D < 5$. The two potentials become indistinguishable for $D > 5$.

3. Dynamic simulations

The cluster potentials can be readily implemented into any computer code employing the MD simulation. Especially for loosely packed assemblies in microscale where the cluster radius is small comparing to the distance between clusters, the change only involves the exponents describing attractions and repulsions, i.e., the values of m and n, and the coefficients A, C_1, C_2, N_1, and N_2 in Eq. (11). The procedures calculating thermal properties of nanoscale assemblies [7–9,26] remain the same, which will appear in our communication in the near future.

To better describe the unique features in cluster dynamics, we model the one-dimensional interactions among N identical spherical clusters. In terms of two general clusters located at x_i and x_j in the one-dimensional array, $i = 1, 2, \ldots, N$, the nondimensional form of equations of motion can be written as

$$\ddot{X}_i = \frac{\mathrm{d}V_i}{\mathrm{d}\tau} = \frac{\mathrm{d}^2X_i}{\mathrm{d}\tau^2} = \sum_{\substack{j=1\\ j\neq i}}^{N} F_{ji}$$

$$= -mn\sum_{\substack{j=1\\ j\neq i}}^{N}\left[\frac{1}{|X_i - X_j|^{m+1}} - \frac{1}{|X_i - X_j|^{n+1}}\right];$$

$$F_{ij} = -F_{ji} \quad \text{where} \quad X = \frac{x}{d_0},$$

$$\tau = \frac{t}{\sqrt{\frac{6Md_0^2}{E_0}}}, \quad V = \frac{v}{d_0/\sqrt{\frac{6Md_0^2}{E_0}}} \tag{17}$$

This version of the nondimensional scheme includes m and n, the exponents describing the attractive and repulsion of the cluster potential. For identical clusters of a spherical shape, as shown in Table 1, $m = 7$ and $n = 1$.

Eq. (17) represents a set of nonlinearly coupled ordinary differential equations to be solved for the cluster displacements (X_i) and velocities (V_i) in the time history. The ODE solver, IVPAG in the IMSL package is used for this purpose. The global tolerance is set to 10^{-6} for achieving convergent numerical integrations in this work. Fig. 6 shows the dynamic behavior of ten (10) identical spherical clusters where the motion is set forth under the following initial conditions:

$$X_i(0) = 1.1(i-1), \quad \dot{X}_i(0) = 0$$
$$\text{for } i = 1, 2, \ldots, 10 \tag{18}$$

Comparing to the classical molecular dynamics simulation shown by the short dashes in Fig. 6, oscillation of clusters occurs at a much lower frequency with a much larger amplitude, which are more evident for clusters near the two ends of the 10-cluster assembly, i.e., clusters no. 1–3 and 8–10. Comparing to the classical molecular dynamics, the lower frequency results from the larger mass of the clusters whereas the larger amplitude results from the larger inertia carried by the clusters in motion. In converting into the physical scales of space and time, note that $x \cong 0.18X$ (nm) and $t \cong 1.26\tau$ (ns), which apply to all results shown in this work.

Maxwell–Boltzmann velocity distribution is a necessary condition for assuring sufficient number of particles employed in the dynamic simulation [9]. In a quasi-stationary response, the time-average of the particle velocity, $\bar{v}$ or $\overline{V}$ defined in Eq. (17), must follow the relation

$$\frac{\Delta N_V}{N} \equiv P = \left(\frac{M}{2\pi k_\mathrm{B}\overline{T}}\right)\exp\left[-\frac{M\bar{v}^2}{2\pi k_\mathrm{B}\overline{T}}\right]\times\Delta\bar{v}$$

$$= \frac{\exp\left(-\frac{\overline{V}^2}{2\bar{\theta}}\right)}{\sqrt{2\pi\bar{\theta}}}\times\Delta\overline{V} \tag{19}$$

Eq. (19) measures the probability of having (ΔN_V) clusters (among the total of N clusters) that have a time-averaged velocity within $\overline{V} + \Delta\overline{V}$. Since the averaged temperature, $\overline{T}$ or $\bar{\theta} = \overline{T}/(E_0/6k_\mathrm{B})$ in Eq. (19), is related to the averaged velocity by

$$\frac{1}{2}Mv^2 = \frac{3}{2}k_\mathrm{B}T, \quad \text{or}$$

$$\bar{\theta} = \frac{\overline{V}^2}{3} \quad \text{in a nondimensional form} \tag{20}$$

the probability is a strong function of the averaged velocity $(\overline{V})$. Fig. 7 shows the evolution of the probability density curve as the number of clusters increases from 10 to 200. Although better agreement with the

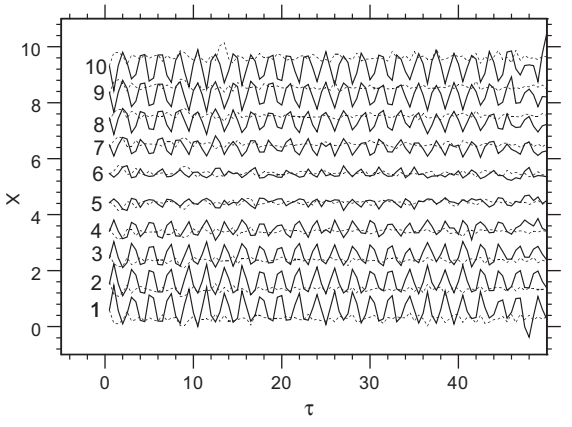

Fig. 6. Dynamic behavior of 10 identical spherical clusters: solid lines represent cluster dynamics and dashed lines represent molecular dynamics.

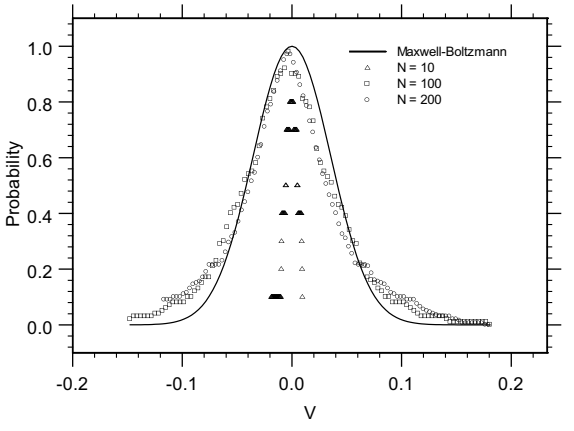

Fig. 7. N clusters approaching the Maxwell–Boltzmann velocity distribution: the cases of $N = 10$, 100, and 200. $X_i(0) = 1.1(i-1)$, $\dot{X}_i(0) = 0$ for $i = 1, 2, \ldots, N$.

Maxwell–Boltzmann distribution can be achieved by the use of more clusters, the case of $N = 100$ may be most cost-effective in view of its close agreement and the computational time that exponentially increases with the number of clusters used in the simulation. In Fig. 7, for $N = 100$, the averaged temperature is $\bar{\theta} = 2.5038 \times 10^{-3}$ and the peak value of the probability is approximately 0.997, which occurs at $\overline{V} = 0$.

Fig. 8(a) shows the dynamic behavior in a nanophase assembly consisting of 100 clusters. Under the same initial conditions described by Eq. (18) with i ranging from 1 to 100 in this case, the first $(i = 1)$ and last $(i = 100)$ cluster are held in place at all times, i.e., $\dot{X}_1(\tau) = 0$ and $\dot{X}_{100}(\tau) = 0$, to simulate bounded motion by rigid confiners. The nonequilibrium behavior, and consequently the nonequilibrium thermomechanical responses discussed later, persists mainly in $\tau < 170$ for all clusters. A quasi-stationary response seems to prevail after $\tau \cong 300$, in the sense that continued oscillations take place around a constant mean for each cluster. This should be the time domain, $\tau > 300$, beyond which steady-state properties such as thermal conductivity [7,8,26], heat capacity [9] (for energy-carrying capacity) or Young's modulus [10] (load-bearing capacity) are estimated from the averaged response of the clusters. Calculations in support of this important task are similar to those employing the MD simulations.

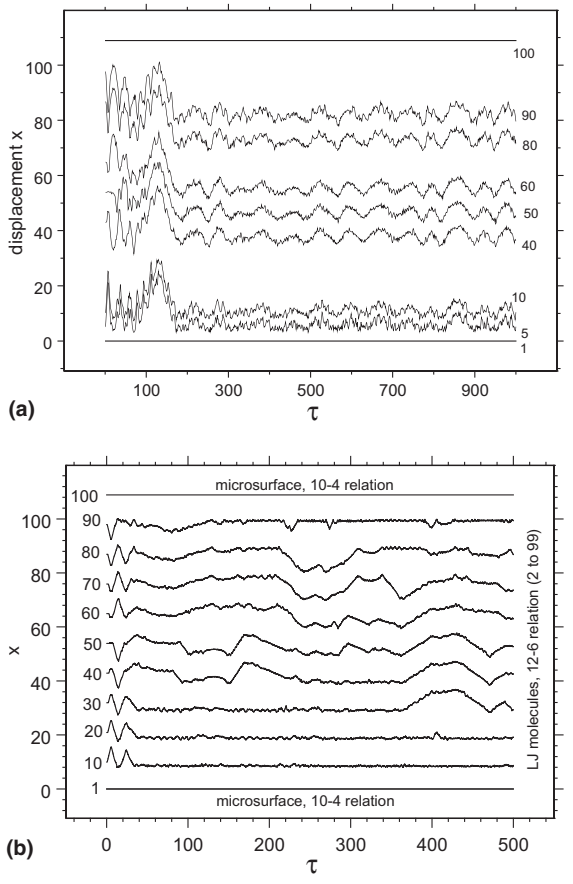

Fig. 8. (a) Dynamic simulation of 100 clusters under the following conditions: $X_i(0) = 1.1(i-1)$ and $\dot{X}_i(0) = 0$ for $i = 1, 2, \ldots, 100$; $\dot{X}_1(\tau) = 0$ and $\dot{X}_{100}(\tau) = 0$. (b) Dynamic simulation of 98 molecules ($i = 2$ to 99) bounded by 2 stationary microsurfaces ($i = 1$ and 100). The ratios $M_0/M = 0.1$, $E/E_0 = 0.93$, and $d_0/d = 1.11$ are used in Eq. (21).

A salient feature in the cluster approach is description of a physical boundary in terms of a *cluster potential* with different exponents and coefficients characterizing attractions and repulsions. An example is given in Fig. 8(b), where 98 molecules ($i = 2$–99 with $m = 12$ and $n = 6$) are bounded by two stationary *planar clusters* ($i = 1$ and 100 with $m = 10$ and $n = 4$) in setting forth their motion. The values of $m = 12$ and $n = 6$ are used in Eq. (17) for the molecular motion governed by the traditional LJ potential, with $i = 2$–98. In describing the interactions involving the first $(i = 1)$ or last $(i = 100)$ planar cluster, the values of m and n are replaced by 10 and 4, respectively, and Eq. (16) is changed to the following form:

$$\ddot{X}_j = -mn\left(\frac{M_0}{M}\right)\left(\frac{E}{E_0}\right)\sum_{\substack{i=1\\ i\neq j}}^{N}\left[\frac{1}{\left(\frac{d_0}{d}\right)^m |X_i - X_j|^{m+1}} - \frac{1}{\left(\frac{d_0}{d}\right)^n |X_i - X_j|^{n+1}}\right];$$
$$m = 10,\ n = 4 \quad \text{for} \quad \text{planar clusters},\ i = 1 \text{ or } N \tag{21}$$

The subscript "0" refers to the molecules (atoms). Eq. (10) involves the mass-ratio of M_0 (mass of molecules) to M (mass of planar clusters), ratio of the potential-well-depth E_0 to E, and the equilibrium-distance-ratio d_0 to d. A physical boundary, two bounded planes in this case, can thus be described by the use of a different cluster potential, along with involvement of the three ratios in the equation of motion. Fig. 8(b) results from the use of $M_0/M = 0.1$, $E/E_0 = 0.93$, and $d_0/d = 1.11$, which are estimated from the potential curves shown in Fig. 4.

Unique capabilities of the cluster model in describing multi-scale interactions now become clear. Different clusters of different shapes, and consequently different exponents characterizing attractions and repulsions, can be introduced to model multi-scale interactions in complex nanostructures. Different clusters are accommodated by a simple change of the attractive and repulsive exponents according to the cluster shape, and involving the various ratios in Eq. (21) is merely straightforward.

4. Conclusion

Cluster potentials have been derived in this work under a wide variety of cluster geometries. The molecular LJ potential has been used as a Green's function to derive the cluster potential analytically. As molecules congregate in different shapes in microscale, the exponents characterizing attractions and repulsions sensitively vary, which may be very different from the 12–6 relation (LJ potential). Dynamic behavior of clusters has been analyzed, with emphasis on the deviations from that driven by the LJ potential on the molecular level. The group behavior of clusters includes a lower frequency, but much larger amplitude as they interact in a nanophase assembly. Salient features of the cluster approach include modeling a physical boundary by a cluster potential with different exponents of attraction and repulsion, which can easily be expanded to include nanostructures with extreme complexities. The cluster potential does involve a longer range of influence, approximately $7–8d_0$ as compared to the $2–3d_0$ in the classical MD simulation. The interaction force over a longer range implies the need for specifying a larger cutoff radius in the dynamic simulation, resulting in a longer computational time that is a counterbalanced effect to the savings from consolidating molecules into clusters. Since the number of participating species (number of clusters versus number of molecules) in the computational domain is the main cause for exhausting the computational time, and only a very limited number of clusters would be required in the longer range of the interaction force due to their larger dimensions, it is anticipated that the saving from the potentially much less clusters involved in the computational domain would suppress the little investment made toward covering the interaction forces over a longer range.

Dynamic simulation performed in this work aims to reveal unique features in the cluster approach, by using the least number of clusters/molecules in the computational domain to reduce the unnecessary complexity. Much more clusters/molecules will be needed to capture detailed behaviors in real devices. The cluster model established in this work, in addition, is only valid for loosely compacted assembly, where the radius of the spherical cluster is small comparing to the distance between two clusters. Should a tightly compacted assembly be considered, radius of the cluster should be considered in the dynamic equations of motion, and a factor of $2A$, with $A = a/d_0$ being the nondimensional radius of identical spheres, needs to be subtracted from $|X_i - X_j|$ in Eq. (17). Along with detailed computations for the thermomechanical properties, including extension of the virial theorem for calculating heat flux and stresses transmitted through clusters, the difference between loosely and tightly compacted assemblies shall be reported in the near future.

References

[1] S.D. Brorson, J.G. Fujimoto, E.P. Ippen, Femtosecond electron heat-transport dynamics in thin gold film, Phys. Rev. Lett. 59 (1987) 1962–1965.
[2] M.I. Flik, C.L. Tien, Size effect on the thermal conductivity of high-T_c thin-film superconductors, ASME J. Heat Transfer 112 (1990) 872–881.
[3] T.Q. Qiu, C.L. Tien, Short-pulse laser heating on metals, Int. J. Heat Mass Transfer 35 (1992) 719–726.
[4] T.Q. Qiu, T. Juhasz, C. Suarez, W.E. Bron, C.L. Tien, Femtosecond laser heating of multi-layered metals—II. Experiments, Int. J. Heat Mass Transfer 37 (1994) 2799–2808.
[5] D.Y. Tzou, J.K. Chen, J.E. Beraun, Ultrafast deformation in femtosecond laser heating, ASME J. Heat Transfer 124 (2002) 284–292.
[6] D.Y. Tzou, J.K. Chen, J.E. Beraun, Hot-electron blast induced by ultrashort-pulsed lasers in layered media, Int. J. Heat Mass Transfer 45 (2002) 3369–3382.
[7] J.R. Lukes, D.Y. Li, X.-G. Liang, C.L. Tien, Molecular dynamics study of solid thin-film thermal conductivity, ASME J. Heat Transfer 122 (2000) 536–543.
[8] X. Wang, X. Xu, Molecular dynamics simulation of heat transfer and phase change during laser material interaction, ASME J. Heat Transfer 124 (2002) 265–274.
[9] Y.S. Xu, D.X. Xiong, D.Y. Tzou, One dimensional molecular dynamics simulation, in: ICHMT Symposium on Molecular and Microscale Heat Transfer in Materials Processing and Other Applications, vol. 1, Yokohama, Japan, 1996, pp. 49–56.
[10] ICHMT Symposium on Molecular and Microscale Heat Transfer in Materials Processing and Other Applications, vols. 1 and 2, Yokohama, Japan, 1996.
[11] F.C. Chou, J.R. Lukes, X.-G. Liang, K. Takahashi, C.L. Tien, Molecular dynamics in microscale thermophysical engineering, in: C.L. Tien (Ed.), Annual Review of Heat Transfer, Begell House, New York, NY, 1999, pp. 141–176.
[12] F.H. Stillinger, T.A. Weber, Computer simulation of local order in condensed phases of silicon, Phys. Rev. B 31 (1985) 5262–5271.
[13] J. Tersoff, New model for the structure properties of silicon, Phys. Rev. Lett. 56 (1986) 632–635.
[14] R. Car, M. Parrinello, Unified approach for MD and density functional theory, Phys. Rev. Lett. 55 (1985) 2471–2474.
[15] A. Debernardi, M. Bernasconi, M. Cardona, M. Parrinello, Infrared absorption in amorphous silicon from ab initio molecular dynamics, Appl. Phys. Lett. 71 (1997) 2692–2694.
[16] S. Kotake, Molecular Thermo-Fluid Dynamics, Maruzen, Japan, 1992.
[17] T. Iwaki, Molecular dynamics study of stress–strain in very thin film (size and location of region defining stress and strain), Jpn. Soc. Mech. Eng. 61A (1995) 319–327.

[18] DOE (Department of Energy) BES (Basic Energy Sciences) Workshop, 1999, Complex Systems—Science for the 21st Century. Available from <www.sc.doe.gov/production/bes/complexsystems.htm>.
[19] DOE (Department of Energy) BES (Basic Energy Sciences) Workshop, 1999, Nanoscale Science, Engineering, and Technology—Research Direction. Available from <www.sc.doe.gov/production/bes/nanoscale.html>.
[20] R.W. Siegel, Creating nanophase materials, Sci. Am. (1996) 74–79.
[21] G.C. Sih, A special theory of crack propagation, in: G.C. Sih (Ed.), Methods of Analysis and Solutions of Crack Problems, Mechanics of Fracture 1, Noordhoff, Leyden, The Netherlands, 1973, pp. XXI–XLV.
[22] D.Y. Tzou, Intensification of externally applied magnetic field around a crack in layered composite, J. Theor. Appl. Fract. Mech. 6 (1985) 191–199.
[23] J.R. Rice, G.F. Rosengren, Plan strain deformation near a crack tip in a power-law hardening material, J. Mech. Phys. Solids 16 (1968) 1–12.
[24] J.W. Hutchinson, Plastic stress and strain fields at a crack tip, J. Mech. Phys. Solids 16 (1968) 337–347.
[25] D.Y. Tzou, Characteristics of thermal and flow behavior in the vicinity of discontinuities, Int. J. Heat Mass Transfer 35 (1992) 481–491.
[26] A.R. Abramson, C.L. Tien, A. Majumdar, Interface and strain effects on the thermal conductivity of heterostructures: a molecular dynamics study, ASME J. Heat Transfer 124 (2002) 963–970.